

This discussion paper is/has been under review for the journal Geoscientific Model Development (GMD). Please refer to the corresponding final paper in GMD if available.

# CLM4-BeTR, a generic biogeochemical transport and reaction module for CLM4: model development, evaluation, and application

J. Tang, W. J. Riley, C. D. Koven, and Z. M. Subin

Department of Climate and Carbon Sciences, Earth Sciences Division, Lawrence Berkeley National Lab (LBL), Berkeley, CA, USA

Received: 7 August 2012 – Accepted: 25 August 2012 – Published: 10 September 2012

Correspondence to: J. Tang (jinyuntang@lbl.gov)

Published by Copernicus Publications on behalf of the European Geosciences Union.

**GMDD**

5, 2705–2744, 2012

**CLM4-BeTR for  
biogeochemical  
reaction and  
transport**

J. Tang et al.

Title Page

Abstract

Introduction

Conclusions

References

Tables

Figures

⏪

⏩

◀

▶

Back

Close

Full Screen / Esc

Printer-friendly Version

Interactive Discussion

## Abstract

To improve regional and global biogeochemistry modeling and climate predictability, we have developed a generic reactive transport module for the land model CLM4 (called CLM4-BeTR (Biogeochemical Transport and Reactions)). CLM4-BeTR represents the transport, interactions, and biotic and abiotic transformations of an arbitrary number of tracers (aka chemical species) in an arbitrary number of phases (e.g. dissolved, gaseous, sorbed, aggregate). An operator splitting approach was employed and consistent boundary conditions were derived for each modeled sub-process. Tracer fluxes, associated with hydrological processes such as surface run-on and run-off, below-ground drainage, and ice to liquid conversion were also computed consistently with the bulk water fluxes calculated by the soil physics module in CLM4. The transport code was evaluated and found to be in good agreement with several analytical test cases. The model was then applied at the Harvard Forest site with a representation of depth-dependent belowground biogeochemistry. The results indicated that, at this site, (1) CLM4-BeTR was able to simulate soil-surface CO<sub>2</sub> effluxes and soil CO<sub>2</sub> profiles accurately; (2) the transient surface CO<sub>2</sub> effluxes calculated based on the tracer transport mechanism were in general not equal to the belowground CO<sub>2</sub> production rates and that their differences varied according to the seasonal cycle of soil physics and biogeochemistry; (3) losses of CO<sub>2</sub> through processes other than surface gas efflux were less than 1 % of the overall soil respiration; and (4) the contributions of root respiration and heterotrophic respiration have distinct temporal signals in surface CO<sub>2</sub> effluxes and soil CO<sub>2</sub> concentrations. The development of CLM4-BeTR will allow detailed comparisons between ecosystem observations and predictions and insights to the modeling of terrestrial biogeochemistry.

### CLM4-BeTR for biogeochemical reaction and transport

J. Tang et al.

[Title Page](#)

[Abstract](#)

[Introduction](#)

[Conclusions](#)

[References](#)

[Tables](#)

[Figures](#)



[Back](#)

[Close](#)

[Full Screen / Esc](#)

[Printer-friendly Version](#)

[Interactive Discussion](#)



## 1 Introduction

The trajectory of ongoing climate change (Intergovernmental Panel on Climate Change (IPCC), 2007) depends strongly on greenhouse gas (e.g. H<sub>2</sub>O, CO<sub>2</sub>, CH<sub>4</sub>, and N<sub>2</sub>O) exchanges between the terrestrial biosphere and atmosphere. Globally, gross terrestrial ecosystem greenhouse gas fluxes are at least an order of magnitude larger than anthropogenic emissions and have strong climate sensitivity, which can lead to positive feedbacks with the atmosphere (e.g. Cox et al., 2000; Torn and Harte, 2006). Thus, accurately modeling terrestrial biogeochemistry is a critical component of earth system models (Friedlingstein et al., 2006).

Much effort has been dedicated to designing terrestrial biogeochemistry models that account for hydrological, energy, and carbon and nitrogen dynamics (e.g. Randerson et al.; 1997; Thornton et al., 2002, 2007; Zhuang et al., 2003; and many others). Many of these existing efforts have used, in each terrestrial gridcell, a single vertically integrated layer for soil biogeochemistry, which we refer to here as a “bucket formulation”, as it is analogous to the single-layer hydrology used in early soil-vegetation-atmosphere transfer (SVAT) models. This formulation is insufficient to resolve the depth-dependent soil biogeochemistry, which depends on interactions between the atmosphere, plants, and soils. A good example for the deficiency of the bucket formulation is the treatment of wetland ebullition of trace gases, such as methane (CH<sub>4</sub>). A sufficient amount of volatile gases produced from different biogeochemical processes needs to accumulate before the gas column becomes unstable such that convection can be triggered to move the gas from the deep soil up to the soil surface quickly. The convection process can vary drastically under different atmospheric and soil physical conditions, with ebullition happening in some cases and not others, despite similar total soil gas pressures (e.g. Tokida et al., 2007). Another example is the characterization of the aerobic and anaerobic environments in soil, which can have large vertical gradients (and horizontal gradients as well) that the bucket models cannot represent, but clearly affect which processes are dominating the soil biogeochemistry (e.g. Tang et al., 2010;

**GMDD**

5, 2705–2744, 2012

### **CLM4-BeTR for biogeochemical reaction and transport**

J. Tang et al.

[Title Page](#)

[Abstract](#)

[Introduction](#)

[Conclusions](#)

[References](#)

[Tables](#)

[Figures](#)

[⏪](#)

[⏩](#)

[◀](#)

[▶](#)

[Back](#)

[Close](#)

[Full Screen / Esc](#)

[Printer-friendly Version](#)

[Interactive Discussion](#)



**CLM4-BeTR for biogeochemical reaction and transport**

J. Tang et al.

[Title Page](#)[Abstract](#)[Introduction](#)[Conclusions](#)[References](#)[Tables](#)[Figures](#)[⏪](#)[⏩](#)[◀](#)[▶](#)[Back](#)[Close](#)[Full Screen / Esc](#)[Printer-friendly Version](#)[Interactive Discussion](#)

5 a system with up to four chemical species ( $\text{CH}_4$ ,  $\text{CO}_2$ ,  $\text{N}_2$ , and  $\text{O}_2$ ) in gaseous and aqueous phases and considered different conceptual structures to enable a hierarchical modeling of methane dynamics. This allowed them to explore how methane dynamics depended on the different processes being represented. Still, processes such as adsorption and desorption were not considered there, because no sportive species such as  $\text{NH}_4^+$  or Dissolved Organic Carbon (DOC) were involved in their study, which are critical for a mechanistic modeling of the nitrogen cycle (e.g. Maggi et al., 2008; Gu et al., 2009).

10 Field studies also indicate that it is important to consider slower processes such as bio-turbation (e.g. Yoo et al., 2011) and cryoturbation (e.g. Kaiser et al., 2007) in order to correctly model biogeochemistry in some terrestrial ecosystems. However, to our knowledge, no current model exists that integrates both slow and fast processes contributing to vertical differences in biogeochemical cycling.

15 As understanding of terrestrial ecosystem processes improve, we face the situation of revising biogeochemistry models to incorporate new processes while not losing the legacy of previous model development (see Schmidt et al., 2011 for a perspective discussion on such needs). This situation motivates the development of a generic model template that can relatively easily accommodate new model structures and processes. To meet this and other challenges discussed above, we present here the development of CLM4-BeTR, which includes a flexible modeling structure of terrestrial ecosystem biogeochemistry and a generic multi-phase reaction and transport capability. CLM4-BeTR is integrated in CLM4 (Oleson et al., 2010), the land model of the Earth System Model CESM1.0, thereby allowing simulations that integrate processes involving plants, soils, ocean, atmosphere, urban areas, and land and sea ice. We organize the paper as follows: Sect. 2 describes model structure and parameterization, numerical methods, and theoretical predictions; Sect. 3 presents site level model evaluations; and Sect. 4 presents an example application. Finally, we conclude with a summary in Sect. 5.

20  
25

## 2 Model description

CLM4-BeTR is designed to use a hierarchy of subsurface biogeochemistry models with different levels of complexity and structures and to couple the biogeochemical processes tightly with the physical processes, such that model predictions are as relevant as possible to what can be measured in field experiments (Fig. 1). Starting from the atmosphere, we consider tracers (i.e. any chemical species of interest) precipitated to the soil surface and plant canopy through both dry and wet atmospheric deposition. Volatile tracers such as CO<sub>2</sub> and water vapor are allowed to pass through stomata and enter leaves. Liquid and solid aqueous tracers are allowed to drip off leaves and onto the soil surface. As in the default CLM4, plant litter falls onto the ground and proceeds through a cascade of decomposition. With the microbially-regulated decomposition of litter-derived organic matter and of plant root exudates, relevant tracers are released into the soil and are allowed to move and interact with flowing water and other chemical tracers through both biogeophysical and biogeochemical pathways. All dissolved tracers are allowed to move out of the soil column when the water is drained away, through both over-surface and sub-surface runoff. Volatile tracers are allowed to evaporate back into the soil pore space and atmosphere, and diffuse between the two. Overall, we tried to make the framework sufficiently general that it can tightly couple the various components of a soil-plant-atmosphere system and track the physical, biophysical, chemical, biochemical, and biological dynamics of an arbitrary number of tracers. With this structure, it will be possible to extend the depth-resolved modeling approach from the soil to the canopy air and connect with the atmospheric chemistry and physics.

Below, we first derive the lumped equations for the reactive transport system. Based on the physical characteristics of the different processes, the operator splitting approach (e.g. Strang, 1968) is applied to solve the governing equations. Consistent boundary conditions are presented for the advective and diffusive transport of tracers. Numerical implementations are also presented for solving the advection and diffusion

## CLM4-BeTR for biogeochemical reaction and transport

J. Tang et al.

[Title Page](#)

[Abstract](#)

[Introduction](#)

[Conclusions](#)

[References](#)

[Tables](#)

[Figures](#)



[Back](#)

[Close](#)

[Full Screen / Esc](#)

[Printer-friendly Version](#)

[Interactive Discussion](#)

equations, followed by descriptions of the methods used to diagnose tracer fluxes associated with belowground water flow.

## 2.1 The governing equation

A general reactive-transport model that considers the transport of multiphase chemical species can be derived from the non-steady mass balance relationship (here for three phases: solid (meaning mineral associated), aqueous, and gaseous):

$$\frac{\partial}{\partial t} (C_s + \theta C_w + \varepsilon C_g) = \frac{\partial}{\partial z} \left( D_s \frac{\partial C_s}{\partial z} \right) + \frac{\partial}{\partial z} \left( \theta D_w \frac{\partial C_w}{\partial z} \right) + \frac{\partial}{\partial z} \left( \theta D_g \frac{\partial C_g}{\partial z} \right) - \frac{\partial u_w C_w}{\partial z} - \frac{\partial u_g C_g}{\partial z} + R \quad (1)$$

where  $C_x$ ,  $x = s, w, g$  (mol tracer  $m^{-3}$ ) are tracer concentrations in solid, aqueous, and gaseous phases, respectively;  $D_x$ ,  $x = s, w, g$  ( $m^2 s^{-1}$ ) are diffusivities for tracers in solid, aqueous, and gaseous phases, respectively;  $u_x$ ,  $x = w, g$  ( $ms^{-1}$ ) are the advective velocities for aqueous and gaseous tracers, respectively, which are provided by the soil physics model;  $\theta$  ( $m^3 m^{-3}$ ) is the water filled soil porosity;  $\varepsilon$  ( $m^3 m^{-3}$ ) is the air filled porosity;  $z$  (m) is the spatial coordinate (positive upward);  $t$  (s) represents time; and  $R$  (mol tracer  $m^{-3} s^{-1}$ ) defines the net tracer production rate at time  $t$  and depth  $z$ . Other soil processes such as erosion (Nearing et al., 1994), aggregation and disaggregation (Heuvelink and Pebesma, 1999), sedimentation transport (Merritt et al., 2003), and bioclogging (e.g. Maggi and Porporato, 2007) could also be incorporated into Eq. (1), provided the soil physical processes are modeled consistently. The tracer movement due to horizontal water flow is treated as a separate process and described in Sect. 2.4.

In Eq. (1), we considered diffusive and advective transport of aqueous and gaseous tracers. The vertical movement of adsorbed ( $s$ ) phase is parameterized as a diffusive process (Koven et al., 2009). The reaction term  $R$  includes both net chemical production inside the soil and fluxes due to plant roots, e.g. autotrophic respiration, exudation,

Title Page

Abstract

Introduction

Conclusions

References

Tables

Figures

⏪

⏩

◀

▶

Back

Close

Full Screen / Esc

Printer-friendly Version

Interactive Discussion



and possible transpiration induced fluxes, e.g.  $\text{NO}_3^-$  uptake through roots (Plhak, 2003) and soil  $\text{CO}_2$  transport through root systems into xylem water (Teskey, 2008).

Equation (1) is sufficiently general that it can represent the transport of any well-defined chemical tracer. For example, by ignoring the transport of water vapor in soil, Eq. (1) is reduced to the soil water budget equation currently implemented in CLM4,

$$\frac{\partial}{\partial t} (C_s + \theta C_w) = -\frac{\partial u_w C_w}{\partial z} - q_T \quad (2)$$

where  $C_s$  and  $C_w$  effectively represent the molar concentrations of ice and liquid water, respectively and  $q_T$  ( $\text{mol water m}^{-3} \text{s}^{-1}$ ) represents the sink of water due to transpiration.

We adopted the fast equilibrium assumption, i.e. equilibrium of tracer concentrations between phases is instantaneously achieved (e.g. Maggi et al., 2008). For instance,  $\text{NH}_3$  is considered to exist in three phases in equilibrium: gaseous, lumped aqueous, and adsorbed solid. The lumped aqueous phase includes both  $\text{NH}_4\text{OH}$  and free  $\text{NH}_4^+$ , whose relative concentrations are determined by the equilibrium stoichiometry



Adopting Eq. (3) enables one to group  $\text{NH}_4\text{OH}$  and  $\text{NH}_4^+$  into a single tracer  $(\text{NH}_4^X)_w$ , which is related to  $\text{NH}_4\text{OH}$  through

$$\left[ (\text{NH}_4^X)_w \right] = k_{\text{NH}_3, \text{NH}_4^+} [\text{NH}_4\text{OH}] \quad (4)$$

where the equilibrium constant  $k_{\text{NH}_3, \text{NH}_4^+}$  (unitless) is a function of pH and temperature.

Further, invoking Henry's law, one has  $[\text{NH}_4\text{OH}] = B [(\text{NH}_3)_g]$ , where  $B$  (unitless) is the Bunsen solubility coefficient. Therefore, we have the bulk concentration of  $\text{NH}_4^X$

$$[\text{NH}_4^X] = \theta \left[ (\text{NH}_4^X)_w \right] + \varepsilon [(\text{NH}_3)_g] + [(\text{NH}_4^+)_\text{ads}] \quad (5)$$

**CLM4-BeTR for biogeochemical reaction and transport**

J. Tang et al.

Title Page

Abstract

Introduction

Conclusions

References

Tables

Figures

⏪

⏩

◀

▶

Back

Close

Full Screen / Esc

Printer-friendly Version

Interactive Discussion



as the single state variable to represent the chemical species related to  $\text{NH}_3$ . In Eq. (5),  $(\text{NH}_4^+)_{\text{ads}}$  is the adsorbed phase that is assumed to be in equilibrium with free  $\text{NH}_4^+$  dissolved in water, with a sorption parameter dependent on pH, soil texture, and soil organic matter content.

5 Similarly, the bulk concentration of  $\text{CO}_2^{\text{X}}$  is defined as

$$\text{CO}_2^{\text{X}} = \theta \left[ (\text{CO}_2^{\text{X}})_{\text{w}} \right] + \varepsilon \left[ (\text{CO}_2)_{\text{g}} \right] = \theta \left( [\text{H}_2\text{CO}_3] + [\text{HCO}_3^-] + [\text{CO}_3^{2-}] \right) + \varepsilon \left[ (\text{CO}_2)_{\text{g}} \right] \quad (6)$$

where the relative concentrations of  $\text{H}_2\text{CO}_3$ ,  $\text{HCO}_3^-$ , and  $\text{CO}_3^{2-}$  are determined by their equilibrium stoichiometry (e.g. Maggi et al., 2008; Gu et al., 2009).

## 2.2 Numerical implementation

10 We used the operator splitting approach to solve Eq. (1), which allowed us to use standard numerical solvers to deal with different processes while maintaining numerical efficiency. We grouped the various processes into three different terms, allowing us to rewrite Eq. (1) as

$$\frac{\partial C_{\text{blk}}}{\partial t} = \text{Dif} + \text{Adv} + R \quad (7)$$

15 where  $C_{\text{blk}}$  ( $\text{mol tracer m}^{-3}$ ) is the bulk tracer concentration, including contributions from all possible phases; Dif, Adv, and  $R$  represent, respectively, the impacts of diffusion, advection, and reaction ( $\text{mol tracer m}^{-3} \text{s}^{-1}$ ).

With the Strang splitting approach (Strang, 1968), Eq. (7) can be represented as

$$C_{\text{blk}}(t + \Delta t) = (\text{Dif}, \Delta t/2) (\text{Adv}, \Delta t/2) (R, \Delta t/2) (\text{Adv}, \Delta t/2) (\text{Dif}, \Delta t/2) \quad (8)$$

20 where  $(x, \Delta t)$  denotes the integration of process  $x$  over a time step  $\Delta t$  (s), using the solution from the previous numerical time step as an initial condition. These integrations are done consecutively from right to left and are formulated using the finite volume method.

Title Page

Abstract

Introduction

Conclusions

References

Tables

Figures

◀

▶

◀

▶

Back

Close

Full Screen / Esc

Printer-friendly Version

Interactive Discussion

## CLM4-BeTR for biogeochemical reaction and transport

J. Tang et al.

[Title Page](#)

[Abstract](#)

[Introduction](#)

[Conclusions](#)

[References](#)

[Tables](#)

[Figures](#)

[⏪](#)

[⏩](#)

[◀](#)

[▶](#)

[Back](#)

[Close](#)

[Full Screen / Esc](#)

[Printer-friendly Version](#)

[Interactive Discussion](#)



The soil physics module in CLM4 provides necessary information to drive the integrals in Eq. (8). The vertical advective velocity of liquid water is obtained by solving the Richards' equation. Aqueous and gaseous tracer diffusivities are computed as a function of soil moisture and soil temperature (Appendix A). The solid phase tracer (including adsorbed phase) diffusion is considered as a much slower process (e.g. Koven et al., 2009), such that it can be separated from Eq. (8) and be conducted after the movement of aqueous and gaseous tracers. Specifically, by writing the diffusion processes in Eq. (8) as  $(Dif, \Delta t/2) = (Dif_s, \Delta t/2) (Dif_{gw}, \Delta t/2)$ , where  $Dif_s$  represents diffusion of solid phase tracer, and  $Dif_{gw}$  represents diffusion of aqueous and gaseous phase tracer, it can then be shown that  $C_{blk}(t + \Delta t) = (Dif_s, \Delta t/2) C_{blk}^*(t + \Delta t) (Dif_{gw}, \Delta t/2)$ , where  $C_{blk}^*(t + \Delta t)$  represents the tracer update due to processes other than solid phase diffusion. Thus, because the temporal updating of the tracer concentration is done iteratively, the solid phase tracer diffusion becomes a process that can be split from others.

### 2.2.1 Diffusive transport

The Crank-Nicolson (e.g. Press et al., 1986) approach was used to solve the diffusion process. In contrast to previous approaches, which only consider the existence of a single water table level (or, more generally, wetting front) and restrict it to the connecting interface between two consecutive grid layers, in this study we allow multiple water table levels to coexist inside the soil (to accommodate the existence of perched water table), and they can be within the grid layer rather than being restricted to the grid interface. However, only one wetting front is allowed to exist in a single grid layer, though our approach is extendable to consider more general cases. Specifically, the incoming flux from layer  $j - 1$  to layer  $j$  ( $j$  increases with depth) is computed as (Fig. 2)

$$F_{j-1 \rightarrow j} = -r_{j-1}^{-1} (aC_j - C_{j-1}) \quad (9)$$

and the outgoing flux from layer  $j$  to layer  $j + 1$  is computed as

$$F_{j \rightarrow j+1} = -r_j^{-1} (C_{j+1} - bC_j) \quad (10)$$

where

$$r_{j-1} = \frac{\Delta z_{j-1}}{2D_{j-1}} + \frac{\Delta z_a}{2D_{j,a}} + \frac{\Delta z_b}{2D_{j,b}} \left( \frac{B_{j-1}\theta_{j-1} + \varepsilon_{j-1}}{B_j\theta_j} \right) \quad (11a)$$

$$r_j = \frac{\Delta z_{j+1}}{2D_{j+1}} + \frac{\Delta z_b}{2D_{j,b}} + \frac{\Delta z_a}{2D_{j,a}} \left( \frac{B_{j+1}\theta_{j+1}}{B_j\theta_j + \varepsilon_j} \right) \quad (11b)$$

$$a = \frac{\Delta z_a}{\Delta z_j} + \frac{\Delta z_b}{\Delta z_j} \left( \frac{B_{j-1}\theta_{j-1} + \varepsilon_{j-1}}{B_j\theta_j} \right) \quad (11c)$$

$$b = \frac{\Delta z_a}{\Delta z_j} \left( \frac{B_{j+1}\theta_{j+1}}{B_j\theta_j + \varepsilon_j} \right) + \frac{\Delta z_b}{\Delta z_j} \quad (11d)$$

Equations (9)–(11) are used to solve the diffusion of aqueous and gaseous tracer, where we used  $C_j = \theta_j C_{w,j} + \varepsilon_j C_{g,j}$  and assumed that transport of the adsorbed phase of the tracer (if it does exist) can be considered separately as justified in the formulation of Eq. (8). When the water table level overlaps the grid interface, Eqs. (9)–(11) become identical to the relationships used in Riley et al. (2011).

## 2.2.2 Advective transport

In order to be consistent with the way that CLM4 updates soil water content, the advection operator is next solved for soil aqueous phase tracers:

$$\theta \frac{\partial C_w}{\partial t} = -\frac{\partial u_w C_w}{\partial z} - \left( q_T + \frac{\partial \theta}{\partial t} \right) C_w \quad (12)$$

Currently, gas advection is accounted for by a pressure adjustment approach (e.g. Tang et al., 2010), such that the gas column is always hydrostatically stable. In future work we will incorporate an explicit Darcy solver for gaseous advection.

Since the soil moisture and water fluxes are updated before the advection of the aqueous tracers, Eq. (12) is solved as

$$\frac{\theta^{n+1}}{\Delta t} (C_w^{n+1} - C_w^n) = U^n - \left( q_T + \frac{\partial \theta}{\partial t} \right)^{n+1} C_w^{n+1} \quad (13)$$

where  $U^n$  is the forward-in-time upstream discretization (Tremback et al., 1987) of the advection term in Eq. (12). In the model, whether a particular aqueous tracer is allowed to move with the transpiration flux  $q_T$  is set prior to runtime. As such, CLM4-BeTR provides a method to assess the importance of transpiration-induced tracer fluxes. For instance, the movement of soil  $\text{CO}_2$  into roots and xylem water (Teskey, 2008) or nutrient uptake in the transpired water flow to meet the plant's nutrient demand (e.g. Plhak, 2003) can be explored with this model structure by further considering relevant storage pools in plant.

### 2.2.3 Trace movement in snow

The tracer movement associated with snow accumulation and melt are computed in a similar way as for aerosols in CLM4 (Oleson et al., 2010). CLM4 assumes the aerosols are uniformly sorbed to the snow particles and redistributes them according to the change of snow mass, while assuming no diffusive movement of those aerosols. CLM4-BeTR also considers tracer movement through both advection and diffusion, with the snow-sorbed tracer being adjusted using the fast equilibrium approximation.

### 2.3 Boundary conditions and surface flux calculation

The top boundary condition for advection is determined by the flux from atmospheric precipitation and canopy dripping, either in the form of snowfall or rainfall, or both. For

**CLM4-BeTR for biogeochemical reaction and transport**

J. Tang et al.

Title Page

Abstract

Introduction

Conclusions

References

Tables

Figures



Back

Close

Full Screen / Esc

Printer-friendly Version

Interactive Discussion



diffusion (including dry deposition), a two-layer model similar to that currently applied for water vapor in CLM4 (Oleson et al., 2010) was adopted, as described below.

We assume the gaseous tracer concentration at the level of the apparent sink (Fig. 3) is computed as

$$C_r = r_T \left( \frac{C_{1,g}}{r_{\text{surf}}} + \frac{C_{i,v}}{r_{\text{veg}}} + \frac{C_a}{r_a} \right) \quad (14)$$

where  $C_{i,v}$  (mol tracer  $\text{m}^{-3}$ ; subscript  $i$  means inside leaf) is the weighted leaf internal gas concentration (including contributions from sunlit and shaded leaves, see Appendix B) of a given tracer;  $C_a$  (mol tracer  $\text{m}^{-3}$ ) is the atmospheric gas concentration; and  $C_{1,g}$  (mol tracer  $\text{m}^{-3}$ ) is the top soil control volume gas concentration. The surface ( $r_{\text{surf}}$ ), vegetation ( $r_{\text{veg}}$ ), and weighted bulk ( $r_T$ ) resistances ( $\text{s m}^{-1}$ ) are defined as

$$r_{\text{surf}} = (r_{a,s} + r_{b,s} + r_{s,s}) + \frac{\Delta z_1}{2D_1(B_1\theta_1 + \varepsilon_1)} \quad (15)$$

$$r_{\text{veg}} = r_{b,v} + r_{s,v} \quad (16)$$

$$r_T = \left( \frac{1}{r_{\text{surf}}} + \frac{1}{r_{\text{veg}}} + \frac{1}{r_a} \right)^{-1} \quad (17)$$

where  $r_{a,s}$  ( $\text{s m}^{-1}$ ) is the aerodynamic resistance inside the canopy air;  $r_{b,s}$  ( $\text{s m}^{-1}$ ) is the soil surface laminar boundary layer resistance;  $r_{s,s}$  ( $\text{s m}^{-1}$ ) is the resistance due to surface litter (Sakaguchi and Zeng, 2009);  $r_a$  ( $\text{s m}^{-1}$ ) is the aerodynamic resistance above the canopy;  $r_{b,v}$  ( $\text{s m}^{-1}$ ) is the leaf boundary layer resistance;  $r_{s,v}$  ( $\text{s m}^{-1}$ ) is the weighted stomatal resistance (Eq. B5 in Appendix B) that includes contributions from sunlit and shaded leaves; and  $\Delta z_1$  (m),  $\theta_1$  ( $\text{m}^{-3}$  water  $\text{m}^{-3}$  soil),  $\varepsilon_1$  ( $\text{m}^3$  air  $\text{m}^{-3}$  soil), and  $D_1$  ( $\text{m}^2 \text{s}^{-1}$ ) are, respectively, the thickness, water filled porosity, air filled porosity, and bulk tracer diffusivity defined for the top soil control volume. A derivation of

**CLM4-BeTR for biogeochemical reaction and transport**

J. Tang et al.

[Title Page](#)

[Abstract](#)

[Introduction](#)

[Conclusions](#)

[References](#)

[Tables](#)

[Figures](#)

[⏪](#)

[⏩](#)

[◀](#)

[▶](#)

[Back](#)

[Close](#)

[Full Screen / Esc](#)

[Printer-friendly Version](#)

[Interactive Discussion](#)



Eq. (15) is provided in Tang and Riley (2012, A mechanistic top boundary condition for modeling air-soil diffusive exchange of a generic volatile tracer: theoretical analysis and application to soil evaporation, under review at Water Resources Research).

The diffusive flux at the soil surface,  $F_{\text{surf}}$  (mol tracer  $\text{m}^{-2} \text{s}^{-1}$ , positive upward), is:

$$F_{\text{surf}} = -\frac{C_r - C_{1,g}}{r_{\text{surf}}} = -\frac{r_T}{r_{\text{surf}}} \left( \frac{C_{i,v}}{r_{\text{veg}}} + \frac{C_a}{r_a} \right) + \frac{C_{1,g}}{r_{\text{surf}}} \left( 1 - \frac{r_T}{r_{\text{surf}}} \right) \quad (18)$$

For a non-vegetated bare soil,  $r_{\text{veg}}$  is set to infinity and  $r_{a,s}$  is set to zero, which leads to the diffusive flux up from the surface:

$$F_{\text{surf}} = -\frac{C_a - C_{1,g}}{r_a + r_{\text{surf}}} \quad (19)$$

The diffusive efflux from the vegetation  $F_{\text{veg}}$  (mol tracer  $\text{m}^{-2} \text{s}^{-1}$ ) is:

$$F_{\text{veg}} = -\frac{C_r - C_{i,v}}{r_{\text{veg}}} = -\frac{r_T}{r_{\text{veg}}} \left( \frac{C_{1,g}}{r_{\text{surf}}} + \frac{C_a}{r_a} \right) + \frac{C_{i,v}}{r_{\text{veg}}} \left( 1 - \frac{r_T}{r_{\text{veg}}} \right) \quad (20)$$

The total diffusive flux of the tracer,  $F_{\text{tot}}$  (mol tracer  $\text{m}^{-2} \text{s}^{-1}$ ), exchanging with the atmosphere is:

$$F_{\text{tot}} = \frac{r_T}{r_a} \left( \frac{C_{1,g}}{r_{\text{surf}}} + \frac{C_{i,v}}{r_{\text{veg}}} \right) - \frac{C_a}{r_a} \left( 1 - \frac{r_T}{r_a} \right) \quad (21)$$

The radiation boundary condition (e.g. Raymond and Kuo, 1984) is applied at the lower boundary. However, since CLM4 has no representation of tracer concentrations in groundwater (Oleson et al., 2010), no tracer, except water, is allowed to enter the hydrologically active soil from the aquifer.

## 2.4 Tracer fluxes diagnostics

CLM4-BeTR diagnoses tracer fluxes through different physical pathways explicitly. Tracers from dry and wet deposition to the soil surface are directly added to the first soil (or snow) layer. During snow melting, the aqueous tracers are moved inside the snow layers consistently with liquid water flow. The total aqueous fluxes reaching the soil surface are partitioned into tracer infiltration and run-off loss in accordance with the partitioning of infiltration and surface run-off of liquid water.

To compute horizontal tracer fluxes inside the soil associated with surface runoff, we assumed that aqueous tracers in the first two soil layers (totaling 4.5 cm thick) are in equilibrium with those in the runoff water. The tracer concentrations in these top two soil layers are then updated accordingly. This approach is clearly an approximation and deserves more attention in subsequent model versions.

In order to compute the tracer loss through sub-surface drainage, the fraction of water removed from each hydrologically active layer is tracked explicitly. This fraction of water loss for a given soil layer is then assumed to be equal to the fraction of aqueous tracer being lost, which is then used to compute tracer loss from that specific soil layer.

In the current version of CLM4-BeTR, tracer fluxes through dew formation and drip from plant-interception are generically included following the way that CLM4 deals with the water fluxes through those processes, but are considered to be zero in the analyses that follow. For volatile tracers, the surface exchange through diffusion is computed using the gradient-based approach described in Sect. 2.3. Transport through parenchyma or arenchyma is formulated as in Riley et al. (2011). Ebullition is represented using the approach described in Tang et al. (2010), which considers the pressure contributed from different volatile tracers while imposing no gas volume thresholds as done in Riley et al. (2011).

Since the physical parameters to drive diffusive and advective transport are formulated as functions of soil moisture and temperature, the physical effects of the freeze-thaw cycle are considered prognostically during tracer transport. The ice fraction

**GMDD**

5, 2705–2744, 2012

### CLM4-BeTR for biogeochemical reaction and transport

J. Tang et al.

[Title Page](#)

[Abstract](#)

[Introduction](#)

[Conclusions](#)

[References](#)

[Tables](#)

[Figures](#)

[⏪](#)

[⏩](#)

[◀](#)

[▶](#)

[Back](#)

[Close](#)

[Full Screen / Esc](#)

[Printer-friendly Version](#)

[Interactive Discussion](#)

## CLM4-BeTR for biogeochemical reaction and transport

J. Tang et al.

Title Page

Abstract

Introduction

Conclusions

References

Tables

Figures

⏪

⏩

◀

▶

Back

Close

Full Screen / Esc

Printer-friendly Version

Interactive Discussion



provided by the soil physics module is used to determine the effective porosity of the aqueous and gaseous phases. Whether a given dissolved tracer can be locked into ice is a property that needs to be set prior to runtime. If so, the change in ice fraction over a time step is used to update the fraction of the dissolved tracer locked into, or lost from, the ice. When the surface soil layer is completely frozen, tracer diffusion to the atmosphere is suppressed. This model feature (not applied in the analyses here) allows us to explore the effect of freeze-thaw cycles on substrate and nutrient availability for plant roots and soil microorganisms, which we will explore in future studies. However, the current version of the model resolves the episodic gas emissions due to changes in effective soil porosity following freeze-thaw events (e.g. Mastepanov et al., 2007).

### 3 Model evaluation and example applications

Below we first describe the strategies used to evaluate CLM4-BeTR, including a comparison of numerical and analytical solutions and a comparison of model outputs with site-level measurements at Harvard Forest (<http://harvardforest.fas.harvard.edu/>). Then we present a simple application to show how the tracer tracking capability can provide new insights into interpretation of tracer concentration and flux measurements and their representation in biogeochemical models such as CLM4.

#### 3.1 Evaluation against analytical solutions

A comparison between the numerical and analytical solutions was conducted to evaluate the accuracy of the 1-D transport simulator integrated in CLM4-BeTR. We used two different analytical solutions to evaluate the code. The two analytical solutions satisfy the 1-D reactive transport equation:

$$\frac{\partial C}{\partial t} = \frac{\partial}{\partial z} \left( D \frac{\partial C}{\partial z} \right) - u \frac{\partial C}{\partial z} \quad (22)$$

with their respective initial conditions and boundary conditions. Here  $D$  is diffusivity, and  $u$  is advection velocity (positive downward). In all comparisons between the numerical and analytical solutions, the diffusivity  $D$  was set to  $10^{-6} \text{ m}^2 \text{ s}^{-1}$  and the advection velocity  $u$  was set to  $10^{-7} \text{ m s}^{-1}$  (which is two orders of magnitude greater than typical vertical liquid water flows computed by CLM4).

For the first analytical solution, a pulse tracer input is imposed at the top of a 1-D column of length  $L$ , resulting in the tracer concentration  $C$  ( $\text{mol m}^{-3}$ ):

$$C = \frac{1}{2} \operatorname{erfc} \left( \frac{z-ut}{2\sqrt{Dt}} \right) + \frac{1}{2} \exp \left( \frac{uz}{D} \right) \operatorname{erfc} \left( \frac{z+ut}{2\sqrt{Dt}} \right) + \left[ 1 + \frac{u}{2D} (2L - z + ut) \right] \cdot \exp \left( \frac{uL}{D} \right) \operatorname{erfc} \left( \frac{2L - z + ut}{2\sqrt{Dt}} \right) - \sqrt{\frac{u^2 t}{\pi D}} \exp \left[ \frac{uL}{D} - \frac{(2L - z + ut)^2}{4Dt} \right] \quad (23)$$

where  $\operatorname{erfc}(x)$  is the complementary error function of  $x$ . For the comparisons, we set  $L = 42.10 \text{ m}$ , corresponding to the maximum depth of the temperature solution currently calculated in CLM4 (computed using Eqs. 6.5–6.7 in Oleson et al., 2010).

For the second analytical solution, the tracer concentration top boundary condition is

$$C(z=0) = C_0 + \sum_{i=1}^2 A_i \exp \left( -\frac{u}{2D} - \frac{\sqrt{2}}{4D} \sqrt{u^2 + \sqrt{u^4 + 16D^2\omega_i^2}} \right) \sin(\omega_i t),$$

which leads to the wave type analytical solution:

$$C = C_0 + \sum_{i=1}^2 A_i \exp \left( -\frac{u}{2D} - \frac{\sqrt{2}}{4D} \sqrt{u^2 + \sqrt{u^4 + 16D^2\omega_i^2}} \right) \cdot \sin \left( \omega_i t - \frac{\sqrt{2}\omega_i z}{\sqrt{u^2 + \sqrt{u^4 + 16D^2\omega_i^2}}} \right) \quad (24)$$

where  $A_i, i = 1, 2$ , (mol tracer  $\text{m}^{-3}$ ) are the amplitudes and  $\omega_i, i = 1, 2$ , ( $\text{s}^{-1}$ ) are the frequencies. For the numerical comparison, we set  $C_0 = 12/23$  mol tracer  $\text{m}^{-3}$ ,  $A_1 = 9/23$  mol tracer  $\text{m}^{-3}$ ,  $A_2 = 2/23$  mol tracer  $\text{m}^{-3}$ ,  $\omega_1 = 2\pi/(365 \times 86400)$   $\text{s}^{-1}$  and  $\omega_2 = 2\pi/86400$   $\text{s}^{-1}$ . The values of parameters  $C_0$ ,  $A_1$ , and  $A_2$  are chosen to ensure that the maximum tracer concentration is 1 mol  $\text{m}^{-3}$ .

### 3.2 Single point evaluation at the harvard forest site

We conducted a single point simulation at the Harvard Forest site with depth dependent C and N dynamics, which includes a vertical discretization of the soil biogeochemistry, a decomposition cascade, and nitrification and denitrification parameterization based on the CENTURY model (Parton et al., 1988; Del Grosso et al., 2000) for the site level evaluation. The tracer transport capability of CLM4-BeTR was used to evaluate the soil biogeochemistry, which provides the relevant tracer fluxes. A total of six tracers were modeled:  $\text{N}_2$ ,  $\text{O}_2$ , Ar,  $\text{CO}_2^X$ ,  $\text{N}_2\text{O}$ , and NO. We spun up the model for 1000 yr using a repeating 57-yr (1948–2004) cycle of meteorological data extracted from the global dataset (Qian et al., 2006). Another 40-yr simulation was then conducted, from which the average of the last 10 yr of model output were compared with the measurements. The measurement data include  $\text{CO}_2$  effluxes (as derived ecosystem respiration) from the AmeriFlux dataset (level 4 ecosystem respiration flux data, from year 1992 to 2006; <http://public.ornl.gov/ameriflux/dataproducts.shtml>) and  $\text{CO}_2$  profiles collected at the site from June 1995 to December 2004 (Davidson et al., 2006). Given the uncertainties in meteorological forcing data, model parameterization, and site-model mismatch, we did not try to match the model predictions to the measurements, which would otherwise involve an intensive practice of data assimilation and uncertainty quantification of CLM4 that is beyond the scope of this study. Rather, we grouped the observed daily  $\text{CO}_2$  eddy flux observations into a single-year time series, and compared it with the simulated 10-yr mean daily fluxes and relevant statistics. Similarly, the measured  $\text{CO}_2$  profiles

## CLM4-BeTR for biogeochemical reaction and transport

J. Tang et al.

Title Page

Abstract

Introduction

Conclusions

References

Tables

Figures



Back

Close

Full Screen / Esc

Printer-friendly Version

Interactive Discussion

were grouped into monthly time steps to form a single-year time series to enable the comparison.

### 3.3 Partitioning of surface CO<sub>2</sub> fluxes with CLM4-BeTR

To illustrate potential applications of CLM4-BeTR, we designed a tagged CO<sub>2</sub> tracer simulation to visualize the relative contributions of different sources to the measured soil surface CO<sub>2</sub> fluxes and soil CO<sub>2</sub> concentrations. Specifically, using the initial conditions provided from the simulations described in Sect. 3.2, we represented the CO<sub>2</sub> originating from three sources: root respiration, soil heterotrophic respiration, and from the atmosphere with three tracers and tracked their temporal and spatial evolutions with CLM4-BeTR. This approach allowed us to partition the predicted soil surface CO<sub>2</sub> fluxes into contributions from these three sources. We then analyzed whether these three sources have distinct signals from the soil surface CO<sub>2</sub> effluxes and soil CO<sub>2</sub> concentrations measured in the field.

## 4 Results and discussions

### 4.1 Evaluation against analytical solutions

Comparisons between numerical and analytical solutions indicate the 1-D transport code accurately (root mean square error are less than 0.01 for all cases) represented tracer transport for both the pulse and wave boundary condition simulations using the CLM4 standard vertical discretization and time step (Fig. 4a, c). Refining the vertical resolution (i.e. halving the grid size in the transformed exponential coordinate system, see Eq. (6.5) in Oleson et al., 2010) indicated the numerical convergence with slightly improved results (Fig. 4b, d), but the improvement is small considering the extra computation and storage requested. These results indicate the transport algorithm for CLM4-BeTR has good accuracy for these test cases. We conclude that the default

## CLM4-BeTR for biogeochemical reaction and transport

J. Tang et al.

[Title Page](#)

[Abstract](#)

[Introduction](#)

[Conclusions](#)

[References](#)

[Tables](#)

[Figures](#)



[Back](#)

[Close](#)

[Full Screen / Esc](#)

[Printer-friendly Version](#)

[Interactive Discussion](#)



CLM4 vertical grid structure and time-step (30 min) is sufficient to produce reasonable model simulations.

## 4.2 Single point evaluation at the Harvard Forest site

5 Simulated mean seasonal cycle of ecosystem respiration was generally in good agreement with the data derived from tower eddy flux measurements (Fig. 5). Starting from April (day 91), the model simulated higher ecosystem respiration than observed, though predicted GPP is close to the measurements (with a linear fitting  $x = 0.88y - 0.8780(\mu\text{molCO}_2\text{m}^{-2}\text{s}^{-1})$ , where  $x$  represents simulated GPP, and  $y$  represents the observed data; data not shown). The overestimation in ecosystem respiration could be from any of the predicted respiratory components, including above ground autotrophic respiration, root autotrophic respiration, and soil heterotrophic respiration.

10 We next integrated the predicted belowground  $\text{CO}_2$  production rate with the transport module in CLM4-BeTR to calculate soil-gas  $\text{CO}_2$  concentrations (Fig. 6). The predicted soil  $\text{CO}_2$  concentrations were generally higher than observed from April through June, in relatively good agreement with observations from July through September, and higher than observed from October through December. It is not clear whether the overestimation in soil  $\text{CO}_2$  concentrations resulted from an overestimation of the  $\text{CO}_2$  production rate in soil heterotrophic respiration or in root autotrophic respiration, or insufficient transport due to incorrect physical forcing, or even some combination that varied with time. However, analyses indicated that the simulated soil temperature was in good agreement with measurement at all four-observation depths (6, 10, 33, and 60 cm), where the soil air samples were taken (Fig. S1). The model simulated soil moisture was higher than observed throughout most of the year (Fig. S2). Hence, according to the way that the soil moisture affects the tracer transport and organic matter decomposition (Andren and Paustian, 1987) in the model, a reasonable hypothesis is that (1) the tracer transport was forced by incorrect soil water dynamics and (2) the soil heterotrophic respiration was overestimated, given that oxygen and organic matter availability were never the limiting factor for soil heterotrophic respiration. Further,

### CLM4-BeTR for biogeochemical reaction and transport

J. Tang et al.

Title Page

Abstract

Introduction

Conclusions

References

Tables

Figures



Back

Close

Full Screen / Esc

Printer-friendly Version

Interactive Discussion



a mass budget analysis of the belowground CO<sub>2</sub> dynamics indicated that, at this site, the CO<sub>2</sub> loss through surface and subsurface runoff is less than 1 % of the total CO<sub>2</sub> produced from belowground respiration.

### 4.3 Partitioning surface CO<sub>2</sub> fluxes

We found the three predicted CO<sub>2</sub> sources (soil heterotrophic respiration, root respiration, and atmospheric CO<sub>2</sub>) differ distinctly in contributing to the overall soil surface CO<sub>2</sub> efflux (Fig. 7a). The atmospheric CO<sub>2</sub> source (denoted by Air) contributed a negligible amount (being two orders of magnitude smaller than the other two sources), indicating, as expected, that the surface CO<sub>2</sub> efflux is dominated by belowground biogeochemical production. In this simulation, the CO<sub>2</sub> produced from soil heterotrophic respiration dominated the total surface efflux, particularly in the non-growing season, when autotrophic root respiration diminished due to reduced vegetation productivity. In addition, due to a tight coupling with soil physics, soil heterotrophic CO<sub>2</sub> production was more temporally variable than root autotrophic respiration. However, we are not sure if such behavior is close to what actually occur in the field.

At the daily time step, small yet significant discrepancies existed between simulated surface CO<sub>2</sub> effluxes and heterotrophic plus autotrophic root CO<sub>2</sub> production rates (Fig. 7b, c). However, more significant discrepancies were identified when the surface CO<sub>2</sub> effluxes and total belowground productions rates were compared at the hourly time scale (Fig. 8a, b). In the growing season (from 1 May to 31 October), we found hourly soil surface CO<sub>2</sub> effluxes were often different from the belowground CO<sub>2</sub> production rate (8b). When the histogram of the relative differences (defined as  $(F_{SR} - SR) / F_{SR} \times 100\%$ , where  $F_{SR}$  ( $\mu\text{molCO}_2\text{m}^{-2}\text{s}^{-1}$ ) is the surface CO<sub>2</sub> efflux and SR ( $\mu\text{molCO}_2\text{m}^{-2}\text{s}^{-1}$ ) is the belowground CO<sub>2</sub> production) were analyzed for the growing season, a slightly asymmetric distribution was identified (Fig. 8c), with the soil surface CO<sub>2</sub> efflux slightly higher (statistically significant at the screen level  $p < 0.01$ ) than the belowground production rate. Further analysis indicated such an asymmetry

## CLM4-BeTR for biogeochemical reaction and transport

J. Tang et al.

Title Page

Abstract

Introduction

Conclusions

References

Tables

Figures

⏪

⏩

◀

▶

Back

Close

Full Screen / Esc

Printer-friendly Version

Interactive Discussion

**CLM4-BeTR for  
biogeochemical  
reaction and  
transport**

J. Tang et al.

[Title Page](#)[Abstract](#)[Introduction](#)[Conclusions](#)[References](#)[Tables](#)[Figures](#)[Back](#)[Close](#)[Full Screen / Esc](#)[Printer-friendly Version](#)[Interactive Discussion](#)

was due to the higher emission than production rate signal in the nighttime (Fig. S3). The relative difference at the hourly scale could be as much as 20 % during the growing season, and up to 80 % during the winter, when freeze-thaw driven episodic emissions occurred (e.g. the peak emission on day 30 in Fig. 8a). When averaged over daily time steps, however, the differences between the surface CO<sub>2</sub> effluxes and belowground production were much smaller and showed a more symmetric distribution around the mean zero (Fig. 8c), supporting the finding that the temporal averaging to time scales larger than 24 h could suppress the strong small time step signals in the measured CO<sub>2</sub> surface efflux (Fig. 7). The large differences at the hourly time scale indicate potential problems associated with the common approach used to infer GPP from eddy covariance NEE measurements (Desai et al., 2008).

Grouping the relative differences into a monthly time step showed there were seasonally systematic biases. In particular, the surface CO<sub>2</sub> effluxes tended to be smaller than belowground production during the thaw period, and vice versa during the freezing period (Fig. 8d). To better understand these seasonally dependent biases, we analyzed hourly time step model predictions for four different three-day periods: the end of January, early May, late July, and late October (Fig. 9). In the thaw season, CO<sub>2</sub> loss through surface and belowground drainage, as well as increased soil gas storage capacity, made the surface CO<sub>2</sub> efflux smaller than the total belowground production rates. However, when temperatures were below freezing (days 28–31 and 300–303), the loss through drainage diminished and the soil gas storage capacity decreased, such that very strong episodic CO<sub>2</sub> emissions can occur during the short-term thaw event between two consecutive freezing events or at the start of the thaw season. Such episodic emissions can be three to four times higher than the CO<sub>2</sub> effluxes during the peak-growing season (Fig. 8a and Fig. 9a), and 20 or more times higher than the actual belowground CO<sub>2</sub> production rate. Field measurements are needed to assess whether our prediction is close to the natural reality. However, similar signals have been observed for CH<sub>4</sub> fluxes in the fields (Song et al., 2012).

**CLM4-BeTR for  
biogeochemical  
reaction and  
transport**

J. Tang et al.

[Title Page](#)[Abstract](#)[Introduction](#)[Conclusions](#)[References](#)[Tables](#)[Figures](#)[Back](#)[Close](#)[Full Screen / Esc](#)[Printer-friendly Version](#)[Interactive Discussion](#)

In accordance with the distinct temporal patterns of CO<sub>2</sub> production rates from soil heterotrophic respiration and autotrophic root respiration (Fig. 7), the resulting CO<sub>2</sub> concentrations from these two sources also showed distinct temporal patterns (Fig. 10). The CO<sub>2</sub> produced from soil heterotrophic respiration persisted at higher levels over a longer fraction of the year than CO<sub>2</sub> from root respiration. However, due to the physical transport of the CO<sub>2</sub> in the soil profile, we found that the location of high CO<sub>2</sub> concentrations usually differed from the CO<sub>2</sub> production hot spots. In addition, when an incorrect top boundary condition or a different root profile was used, the simulated surface CO<sub>2</sub> effluxes would not change significantly although the soil CO<sub>2</sub> concentrations would drastically change (results not shown). These findings indicate that field soil CO<sub>2</sub> concentration measurements can provide additional constraints on belowground biogeochemistry besides that provided from surface CO<sub>2</sub> efflux measurements.

## 5 Summary

In this study, we presented methods, testing, and an application of CLM4-BeTR, a general multi-phase reactive transport model integrated in CLM4. The model is designed to tightly couple depth-dependent biogeochemistry and physics, to use a hierarchy of biogeochemistry models with different structural complexities, and to readily couple with atmospheric chemistry and physics modules. The comparison with analytical solutions showed the transport calculations were accurate with the default CLM4 time-step and vertical grid structure. An evaluation of modeled surface CO<sub>2</sub> effluxes and soil CO<sub>2</sub> profiles indicates that the model was able to reasonably capture the seasonal dynamics of soil surface CO<sub>2</sub> effluxes and soil CO<sub>2</sub> concentrations, subject to the uncertainties associated with the measurements and model forcings. The component-wise CO<sub>2</sub> tracer transport experiment indicated that there are timescale-dependent biases between the surface CO<sub>2</sub> effluxes and the corresponding belowground CO<sub>2</sub> production rates. These results indicate that soil CO<sub>2</sub> concentration profile measurements provide additional information beyond soil surface CO<sub>2</sub> efflux measurements to constrain

terrestrial biogeochemistry models (more detailed analyses will be conducted in follow-up studies). In future studies, we will present further developments associated with CLM4-BeTR, such as explicit carbon and nitrogen transport, isotope transport and microbial dynamics, that enable a comprehensive and mechanistically-based evaluation of atmosphere-biosphere interactions, involving both physical and chemical feedbacks.

## Appendix A

### Computing the diffusivities

Following the approach by Moldrup et al. (2003), the effective diffusivity for aqueous tracer is computed as

$$D_w = D_w^* \theta \left( \frac{\theta}{\varphi} \right)^{\kappa/3-1} \quad (\text{A1})$$

The effective diffusivity for gaseous tracer is computed as

$$D_g = D_g^* \varepsilon \left( \frac{\varepsilon}{\varphi} \right)^{3/\kappa} \quad (\text{A2})$$

Here,  $\varphi$  ( $\text{m}^3 \text{m}^{-3}$ ) is the effective soil porosity, being equal to the soil porosity minus the space occupied by ice.  $\kappa$  (unitless) is the shape parameter for the Clapp-Hornberger parameterization (Clapp and Hornberg, 1978).  $D_w^*$  is the aqueous tracer diffusivity in liquid water, and  $D_g^*$  is the gaseous tracer diffusivity in air.

Title Page

Abstract

Introduction

Conclusions

References

Tables

Figures

⏪

⏩

◀

▶

Back

Close

Full Screen / Esc

Printer-friendly Version

Interactive Discussion



## Appendix B

### Computing the weighted leaf internal gas concentration

The flux (positive upward) over the sunlit leaf is

$$F_{\text{sun}} = -r_{\text{sun}}^{-1} (C_{i,\text{sun}} - C_r) \quad (\text{B1})$$

5 and the flux over the shaded leaf is

$$F_{\text{sha}} = -r_{\text{sha}}^{-1} (C_{i,\text{sha}} - C_r) \quad (\text{B2})$$

where the sunlit ( $r_{\text{sun}}$ ) and shaded ( $r_{\text{sha}}$ ) resistance ( $\text{sm}^{-1}$ ) are functions of leaf (stem) area index and leaf boundary layer resistance (see Sect. 5.3 in Oleson et al., 2010).

Then the total flux over the canopy is

$$10 F_{\text{veg}} = F_{\text{sun}} + F_{\text{sha}} = - \left( r_{\text{sun}}^{-1} + r_{\text{sha}}^{-1} \right)^{-1} \left( \frac{r_{\text{sun}}^{-1} C_{i,\text{sun}} + r_{\text{sha}}^{-1} C_{i,\text{sha}}}{r_{\text{sun}}^{-1} + r_{\text{sha}}^{-1}} - C_r \right) \quad (\text{B3})$$

which gives the weighted leaf internal tracer concentration as

$$C_{i,v} = \frac{r_{\text{sun}}^{-1} C_{i,\text{sun}} + r_{\text{sha}}^{-1} C_{i,\text{sha}}}{r_{\text{sun}}^{-1} + r_{\text{sha}}^{-1}} \quad (\text{B4})$$

From Eq. (B3), the weighted stomatal resistance  $r_{s,v}$  ( $\text{sm}^{-1}$ ) is found as

$$r_{s,v} = \left( \frac{1}{r_{\text{sun}}} + \frac{1}{r_{\text{sha}}} \right)^{-1} \quad (\text{B5})$$

15 **Supplementary material related to this article is available online at:**  
<http://www.geosci-model-dev-discuss.net/5/2705/2012/gmdd-5-2705-2012-supplement.pdf>.

Title Page

Abstract

Introduction

Conclusions

References

Tables

Figures

⏪

⏩

◀

▶

Back

Close

Full Screen / Esc

Printer-friendly Version

Interactive Discussion



*Acknowledgements.* This research was supported by the Director, Office of Science, Office of Biological and Environmental Research of the US Department of Energy under Contract No. DE-AC02-05CH11231 as part of their Regional and Global Climate Modeling Program. The authors appreciate Ms. Kathleen Savage and Eric Davidson at the Woods Hole Research Center for providing the soil CO<sub>2</sub> profile data and soil moisture and temperature data at the Harvard Forest site.

## References

- Andren, O. and Paustian, K.: Barley straw decomposition in the field – a comparison of models, *Ecology*, 68, 1190–1200, 1987.
- Clapp, R. B. and Hornberger, G. M.: Empirical equations for some soil hydraulic properties, *Water Resour. Res.*, 14, 601–604, 1978.
- Cox, P. M., Betts, R. A., Jones, C. D., Spall, S. A., and Totterdell, I. J.: Acceleration of global warming due to carbon-cycle feedbacks in a coupled climate model, *Nature*, 408, 184–187, doi:10.1038/35041539, 2000.
- Davidson, E. A., Savage, K. E., Trumbore, S. E., and Borken, W.: Vertical partitioning of CO<sub>2</sub> production within a temperate forest soil, *Glob. Change Biol.*, 12, 944–956, doi:10.1111/J.1365-2486.2005.01142.X, 2006.
- Del Grosso, S. J., Parton, W. J., Mosier, A. R., Ojima, D. S., Kulmala, A. E., and Phongpan, S.: General model for N<sub>2</sub>O and N-2 gas emissions from soils due to denitrification, *Global Biogeochem. Cy.*, 14, 1045–1060, 2000.
- Desai, A. R., Richardson, A. D., Moffat, A. M., Kattge, J., Hollinger, D. Y., Barr, A., Falge, E., Noormets, A., Papale, D., Reichstein, M., and Stauch, V. J.: Cross-site evaluation of eddy covariance GPP and RE decomposition techniques, *Agr. Forest Meteorol.*, 148, 821–838, doi:10.1016/J.Agrformet.2007.11.012, 2008.
- Fang, C. and Moncrieff, J. B.: A model for soil CO<sub>2</sub> production and transport, 1: model development, *Agr. Forest Meteorol.*, 95, 225–236, 1999.
- Friedlingstein, P., Cox, P., Betts, R., Bopp, L., Von Bloh, W., Brovkin, V., Cadule, P., Doney, S., Eby, M., Fung, I., Bala, G., John, J., Jones, C., Joos, F., Kato, T., Kawamiya, M., Knorr, W., Lindsay, K., Matthews, H. D., Raddatz, T., Rayner, P., Reick, C., Roeckner, E., Schnitzler, K. G., Schnur, R., Strassmann, K., Weaver, A. J., Yoshikawa, C., and Zeng, N.: Climate-

**GMDD**

5, 2705–2744, 2012

## CLM4-BeTR for biogeochemical reaction and transport

J. Tang et al.

Title Page

Abstract

Introduction

Conclusions

References

Tables

Figures

⏪

⏩

◀

▶

Back

Close

Full Screen / Esc

Printer-friendly Version

Interactive Discussion

## CLM4-BeTR for biogeochemical reaction and transport

J. Tang et al.

[Title Page](#)

[Abstract](#)

[Introduction](#)

[Conclusions](#)

[References](#)

[Tables](#)

[Figures](#)

[⏪](#)

[⏩](#)

[◀](#)

[▶](#)

[Back](#)

[Close](#)

[Full Screen / Esc](#)

[Printer-friendly Version](#)

[Interactive Discussion](#)



carbon cycle feedback analysis: results from the C(4)MIP model intercomparison, *J. Clim.*, 19, 3337–3353, 2006.

Grant, R. F.: Simulation-model of soil compaction and root-growth, 1. Model structure, *Plant Soil*, 150, 1–14, 1993.

5 Grant, R. F. and Roulet, N. T.: Methane efflux from boreal wetlands: theory and testing of the ecosystem model Ecosys with chamber and tower flux measurements, *Global Biogeochem. Cy.*, 16, 1054, doi:10.1029/2001gb001702, 2002.

10 Gu, C. H., Maggi, F., Riley, W. J., Hornberger, G. M., Xu, T., Oldenburg, C. M., Spycher, N., Miller, N. L., Venterea, R. T., and Steefel, C.: Aqueous and gaseous nitrogen losses induced by fertilizer application, *J. Geophys. Res.-Biogeo.*, 114, G01006, doi:10.1029/2008jg000788, 2009.

Heuvelink, G. B. M. and Pebesma, E. J.: Spatial aggregation and soil process modelling, *Geoderma*, 89, 47–65, 1999.

15 Intergovernmental Panel on Climate Change (IPCC): Climate Change 2007: The Physical Science Basis. Contribution of Working Group I to the Fourth Assessment Report of the Intergovernmental Panel on Climate Change, edited by: Solomon, S., Qin, D., Manning, M., Chen, Z., Marquis, M., Averyt, K. B., Tignor, M., and Miller, H. L., Cambridge University Press, Cambridge, UK and New York, NY, USA, 2007.

20 Kaiser, C., Meyer, H., Biasi, C., Rusalimova, O., Barsukov, P., and Richter, A.: Conservation of soil organic matter through cryoturbation in arctic soils in Siberia, *J. Geophys. Res.-Biogeo.*, 112, G02017, doi:10.1029/2006jg000258, 2007.

Kelly, R. H., Parton, W. J., Crocker, G. J., Grace, P. R., Klir, J., Korschens, M., Poulton, P. R., and Richter, D. D.: Simulating trends in soil organic carbon in long-term experiments using the century model, *Geoderma*, 81, 75–90, 1997.

25 Koven, C., Friedlingstein, P., Ciais, P., Khvorostyanov, D., Krinner, G., and Tarnocai, C.: On the formation of high-latitude soil carbon stocks: effects of cryoturbation and insulation by organic matter in a land surface model, *Geophys. Res. Lett.*, 36, L21501, doi:10.1029/2009gl040150, 2009.

Maggi, F. and Porporato, A.: Coupled moisture and microbial dynamics in unsaturated soils, *Water Resour. Res.*, 43, W07444, doi:10.1029/2006wr005367, 2007.

30 Maggi, F., Gu, C., Riley, W. J., Hornberger, G. M., Venterea, R. T., Xu, T., Spycher, N., Steefel, C., Miller, N. L., and Oldenburg, C. M.: A mechanistic treatment of the dominant

## CLM4-BeTR for biogeochemical reaction and transport

J. Tang et al.

[Title Page](#)

[Abstract](#)

[Introduction](#)

[Conclusions](#)

[References](#)

[Tables](#)

[Figures](#)



[Back](#)

[Close](#)

[Full Screen / Esc](#)

[Printer-friendly Version](#)

[Interactive Discussion](#)

soil nitrogen cycling processes: model development, testing, and application, *J. Geophys. Res.*, 113, G02016, doi:10.1029/2007jg000578, 2008.

Mastepanov, M., Sigsgaard, C., Dlugokencky, E. J., Houweling, S., Strom, L., Tamstorf, M. P., and Christensen, T. R.: Large tundra methane burst during onset of freezing, *Nature*, 456, 628–U658, doi:10.1038/Nature07464, 2008.

Merritt, W. S., Letcher, R. A., and Jakeman, A. J.: A review of erosion and sediment transport models, *Environmental Modell. Softw.*, 18, 761–799, doi:10.1016/S1364-8152(03)00078-1, 2003.

Moldrup, P., Olesen, T., Komatsu, T., Yoshikawa, S., Schjønning, P., and Rolston, D. E.: Modeling diffusion and reaction in soils: X. A unifying model for solute and gas diffusivity in unsaturated soil, *Soil Sci.*, 168, 321–337, doi:10.1097/01.ss.0000070907.55992.3c, 2003.

Nearing, M. A., Lane, L. J., and Lopes, V. L.: Modeling soil erosion, in: *Soil Erosion Research Methods*, edited by: Lal, R., Soil and Water Conservation Society, Ankeny, 127–156, 1994.

Oleson, K. W., Lawrence, D. M., Bonan, G. B., Flanner, M. G., Kluzek, E., Lawrence, P. J., Levis, S., Swenson, S. C., Thornton, P. E., Dai, A., Decker, M., Dickinson, R., Feddes, J., Heald, C. L., Hoffman, F., Lamarque, J., Mahowald, N., Niu, G., Qian, T., Randerson, J., Running, S., Sakaguchi, K., Slater, A., Stockli, R., Wang, A., Yang, Z., Zeng, X., and Zeng, X.: Technical Description of Version 4.0 of the Community Land Model, *Natl. Cent. for Atmos. Res.*, Boulder, CO, 2010.

Parton, W. J., Stewart, J. W. B., and Cole, C. V.: Dynamics of C, N, P and S in grassland soils – a model, *Biogeochemistry*, 5, 109–131, 1988.

Plhak, F.: Nitrogen supply through transpiration mass flow can limit nitrogen nutrition of plants, *Plant Soil Environ.*, 49, 473–479, 2003.

Potter, C., Klooster, S., Myneni, R., Genovese, V., Tan, P. N., and Kumar, V.: Continental-scale comparisons of terrestrial carbon sinks estimated from satellite data and ecosystem modeling 1982–1998, *Global Planet. Change*, 39, 201–213, doi:10.1016/J.Gloplacha.2003.07.001, 2003.

Press, W. H., Flannery, B. P., Teukolsky, S. A., and Vetterling, W. T.: *Numerical Recipes*, Cambridge University Press, New York, 1986.

Qian, T. T., Dai, A., Trenberth, K. E., and Oleson, K. W.: Simulation of global land surface conditions from 1948 to 2004. Part I: Forcing data and evaluations, *J. Hydrometeorol.*, 7, 953–975, 2006.

## CLM4-BeTR for biogeochemical reaction and transport

J. Tang et al.

[Title Page](#)

[Abstract](#)

[Introduction](#)

[Conclusions](#)

[References](#)

[Tables](#)

[Figures](#)

[⏪](#)

[⏩](#)

[◀](#)

[▶](#)

[Back](#)

[Close](#)

[Full Screen / Esc](#)

[Printer-friendly Version](#)

[Interactive Discussion](#)



Randerson, J. T., Thompson, M. V., Conway, T. J., Fung, I. Y., and Field, C. B.: The contribution of terrestrial sources and sinks to trends in the seasonal cycle of atmospheric carbon dioxide, *Global Biogeochem. Cy.*, 11, 535–560, 1997.

Raymond, W. H. and Kuo, H. L.: A radiation boundary-condition for multi-dimensional flows, *Q. J. Roy. Meteor. Soc.*, 110, 535–551, 1984.

Riley, W. J.: A modeling study of the impact of the delta  $\delta^{18}\text{O}$  value of near-surface soil water on the delta  $\delta^{18}\text{O}$  value of the soil-surface  $\text{CO}_2$  flux, *Geochim Cosmochim. Ac.*, 69, 1939–1946, doi:10.1016/J.Gca.2004.10.021, 2005.

Riley, W. J., Subin, Z. M., Lawrence, D. M., Swenson, S. C., Torn, M. S., Meng, L., Mahowald, N. M., and Hess, P.: Barriers to predicting changes in global terrestrial methane fluxes: analyses using CLM4Me, a methane biogeochemistry model integrated in CESM, *Biogeosciences*, 8, 1925–1953, doi:10.5194/bg-8-1925-2011, 2011.

Sakaguchi, K., and Zeng, X. B.: Effects of soil wetness, plant litter, and under-canopy atmospheric stability on ground evaporation in the Community Land Model (CLM3.5), *J. Geophys. Res.-Atmos.*, 114, D01107, doi:10.1029/2008jd010834, 2009.

Schmidt, M. W., Torn, M. S., Abiven, S., Dittmar, T., Guggenberger, G., Janssens, I. A., Kleber, M., Kogel-Knabner, I., Lehmann, J., Manning, D. A., Nannipieri, P., Rasse, D. P., Weiner, S., and Trumbore, S. E.: Persistence of soil organic matter as an ecosystem property, *Nature*, 478, 49–56, doi:10.1038/nature10386, 2011.

Simunek, J. and Suarez, D. L.: Modeling of carbon-dioxide transport and production in soil. 1. Model development, *Water Resour. Res.*, 29, 487–497, 1993.

Song, C., Xu, X., Sun, X., Tian, H., Miao, Y., Wang, X., and Guo, Y.: Large methane emission upon spring thaw from natural wetlands in the northern permafrost region, *Environ. Res. Lett.*, 7, doi:10.1088/1748-9326/7/3/034009, 2012.

Strang, G.: On Construction and Comparison of Difference Schemes, *Siam J. Numer. Anal.*, 5, 506–517, 1968.

Tang, J., Zhuang, Q., Shannon, R. D., and White, J. R.: Quantifying wetland methane emissions with process-based models of different complexities, *Biogeosciences*, 7, 3817–3837, doi:10.5194/bg-7-3817-2010, 2010.

Teskey, R. O., Saveyn, A., Steppe, K., and McGuire, M. A.: Origin, fate and significance of  $\text{CO}_2$  in tree stems, *New Phytologist*, 177, 17–32, doi:10.1111/J.1469-8137.2007.02286.X, 2008.

Thornton, P. E., Law, B. E., Gholz, H. L., Clark, K. L., Falge, E., Ellsworth, D. S., Golstein, A. H., Monson, R. K., Hollinger, D., Falk, M., Chen, J., and Sparks, J. P.: Modeling and measuring

## CLM4-BeTR for biogeochemical reaction and transport

J. Tang et al.

[Title Page](#)

[Abstract](#)

[Introduction](#)

[Conclusions](#)

[References](#)

[Tables](#)

[Figures](#)

[⏪](#)

[⏩](#)

[◀](#)

[▶](#)

[Back](#)

[Close](#)

[Full Screen / Esc](#)

[Printer-friendly Version](#)

[Interactive Discussion](#)

the effects of disturbance history and climate on carbon and water budgets in evergreen needleleaf forests, *Agr. Forest Meteorol.*, 113, 185–222, 2002.

Thornton, P. E., Lamarque, J.-F., Rosenbloom, N. A., and Mahowald, N. M.: Influence of carbon-nitrogen cycle coupling on land model response to CO<sub>2</sub> fertilization and climate variability, *Global Biogeochem. Cy.*, 21, GB4018, doi:10.1029/2006gb002868, 2007.

Tokida, T., Mizoguchi, M., Miyazaki, T., Kagemoto, A., Nagata, O., and Hatano, R.: Episodic release of methane bubbles from peatland during spring thaw, *Chemosphere*, 70, 165–171, doi:10.1016/J.Chemosphere.2007.06.042, 2007.

Torn, M. S. and Harte, J.: Missing feedbacks, asymmetric uncertainties, and the underestimation of future warming, *Geophys. Res. Lett.*, 33, L10703, doi:10.1029/2005gl025540, 2006.

Tremback, C. J., Powell, J., Cotton, W. R., and Pielke, R. A.: The forward-in-time upstream advection scheme – extension to higher orders, *Month. Weather Rev.*, 115, 540–555, 1987.

Walter, B. P. and Heimann, M.: A process-based, climate-sensitive model to derive methane emissions from natural wetlands: application to five wetland sites, sensitivity to model parameters, and climate, *Global Biogeochem. Cy.*, 14, 745–765, 2000.

Wania, R., Ross, I., and Prentice, I. C.: Implementation and evaluation of a new methane model within a dynamic global vegetation model: LPJ-WHyMe v1.3.1, *Geosci. Model Dev.*, 3, 565–584, doi:10.5194/gmd-3-565-2010, 2010.

Yoo, K., Ji, J. L., Aufdenkampe, A., and Klaminder, J.: Rates of soil mixing and associated carbon fluxes in a forest versus tilled agricultural field: implications for modeling the soil carbon cycle, *J. Geophys. Res.-Biogeo.*, 116, G01014, doi:10.1029/2010jg001304, 2011.

Zhuang, Q., McGuire, A. D., Melillo, J. M., Clein, J. S., Dargaville, R. J., Kicklighter, D. W., Myneni, R. B., Dong, J., Romanovsky, V. E., Harden, J., and Hobbie, J. E.: Carbon cycling in extratropical terrestrial ecosystems of the Northern Hemisphere during the 20th century: a modeling analysis of the influences of soil thermal dynamics, *Tellus B*, 55, 751–776, 2003.

**CLM4-BeTR for biogeochemical reaction and transport**

J. Tang et al.

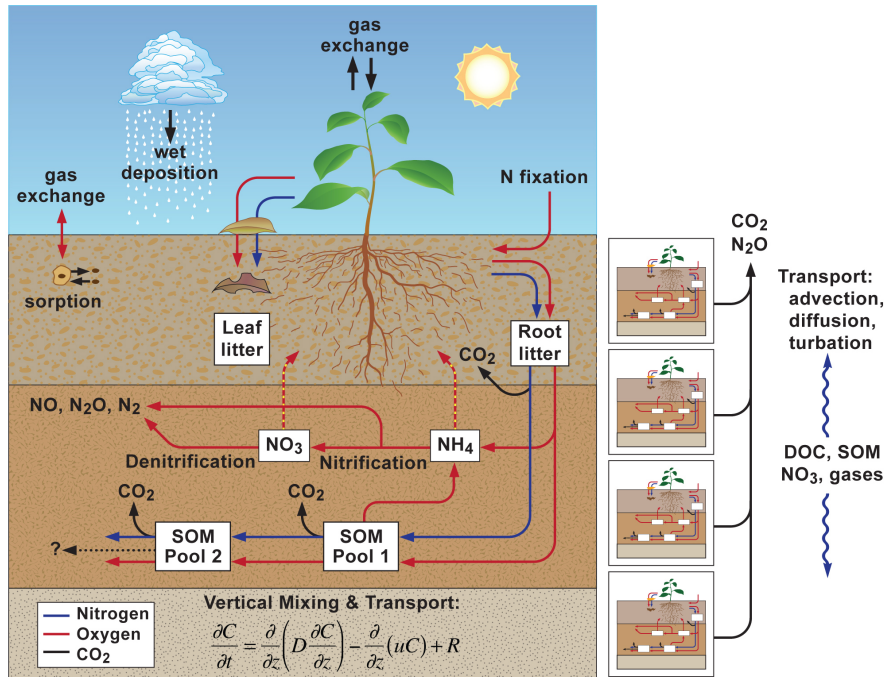


**Fig. 1.** Model structure of CLM4-BeTR: the example is based on the carbon and nitrogen cycles.

Title Page	
Abstract	Introduction
Conclusions	References
Tables	Figures
◀	▶
◀	▶
Back	Close
Full Screen / Esc	
Printer-friendly Version	
Interactive Discussion	

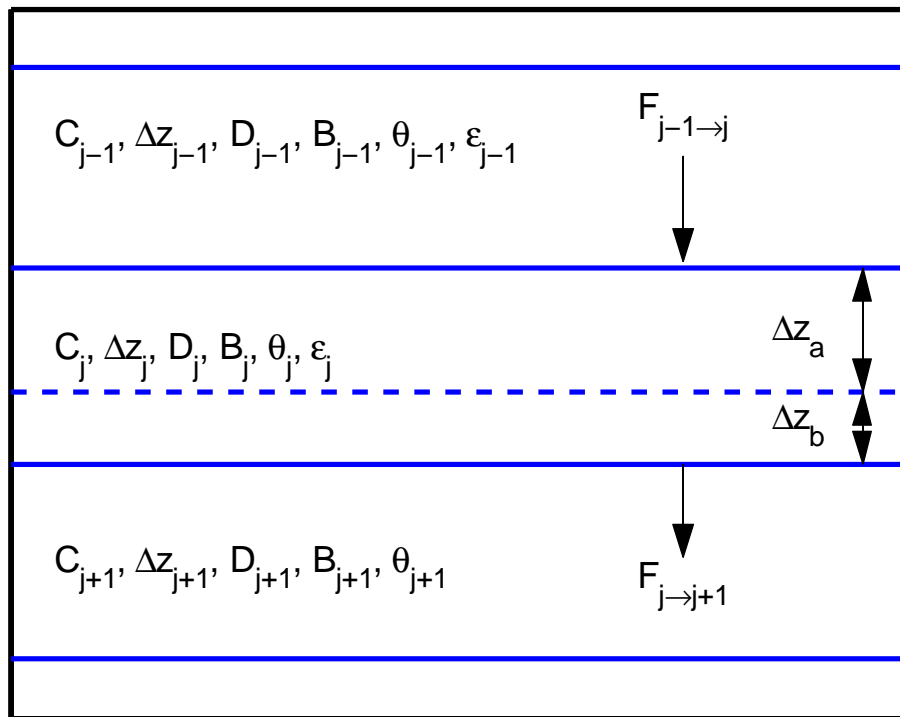


**Fig. 2.** Numerical model configuration when the water table (dashed line) is inside a grid layer. Three grid layers are considered:  $j - 1$ ,  $j$ , and  $j + 1$ . Relevant symbols are defined in the text.

**CLM4-BeTR for biogeochemical reaction and transport**

J. Tang et al.

<a href="#">Title Page</a>	
<a href="#">Abstract</a>	<a href="#">Introduction</a>
<a href="#">Conclusions</a>	<a href="#">References</a>
<a href="#">Tables</a>	<a href="#">Figures</a>
<a href="#">⏪</a>	<a href="#">⏩</a>
<a href="#">◀</a>	<a href="#">▶</a>
<a href="#">Back</a>	<a href="#">Close</a>
<a href="#">Full Screen / Esc</a>	
<a href="#">Printer-friendly Version</a>	
<a href="#">Interactive Discussion</a>	



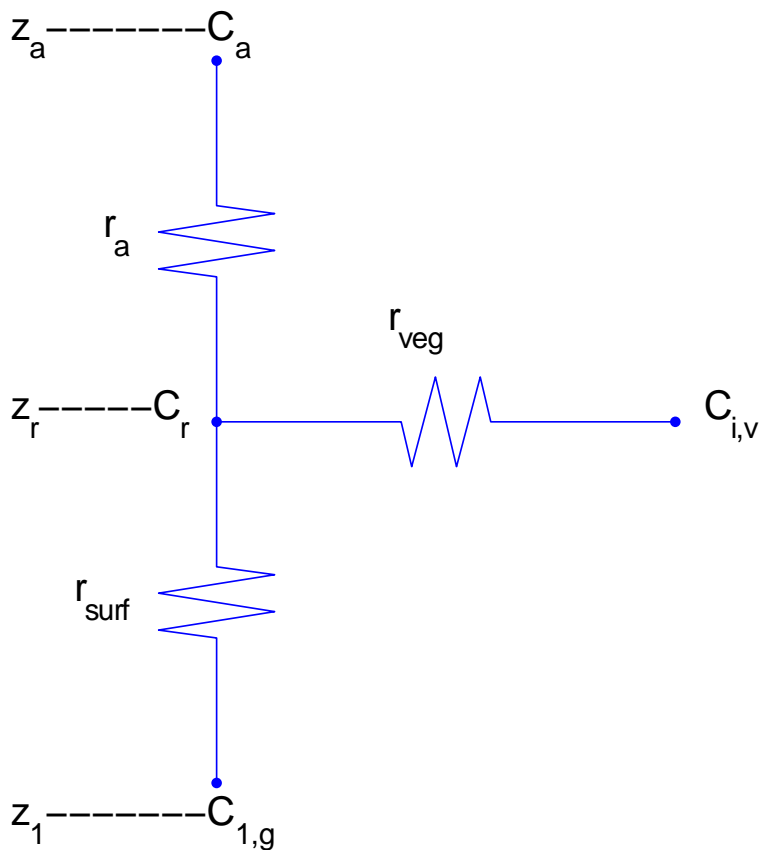


**Fig. 3.** The relationship between gas concentrations at different levels (i.e.,  $z_1$  is the center of the top soil control volume,  $z_r$  is the apparent sink level, and  $z_a$  is the atmosphere reference height) and their relevant resistances. The relationships are explained in text.

Title Page

Abstract

Introduction

Conclusions

References

Tables

Figures

◀

▶

◀

▶

Back

Close

Full Screen / Esc

Printer-friendly Version

Interactive Discussion

## CLM4-BeTR for biogeochemical reaction and transport

J. Tang et al.

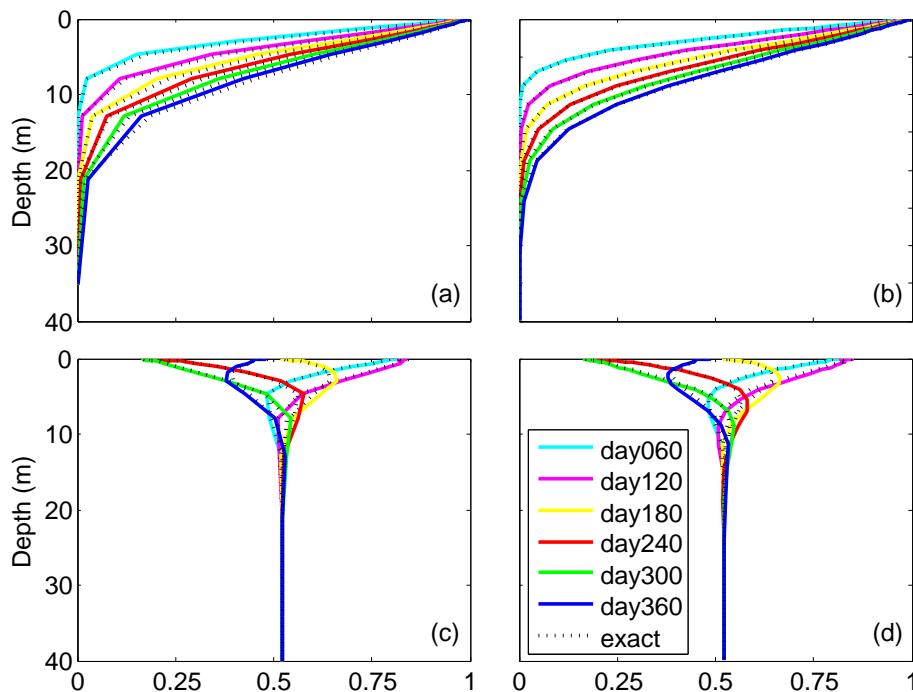


**Fig. 4.** Comparison between analytical (denoted as exact in the figure) and numerical solutions: **(a)** and **(b)** are for the pulse type solution described in Eq. (23); **(c)** and **(d)** are for the wave type solution described in Eq. (24). The left panels used the standard transformed exponential discretization for a soil column in CLM4 (see Eq. (6.5) in Oleson et al., 2010). The right panels used a refined discretization by doubling the number of nodes in the transformed exponential grid. See text for details of the comparison.

Title Page

Abstract

Introduction

Conclusions

References

Tables

Figures

⏪

⏩

◀

▶

Back

Close

Full Screen / Esc

Printer-friendly Version

Interactive Discussion

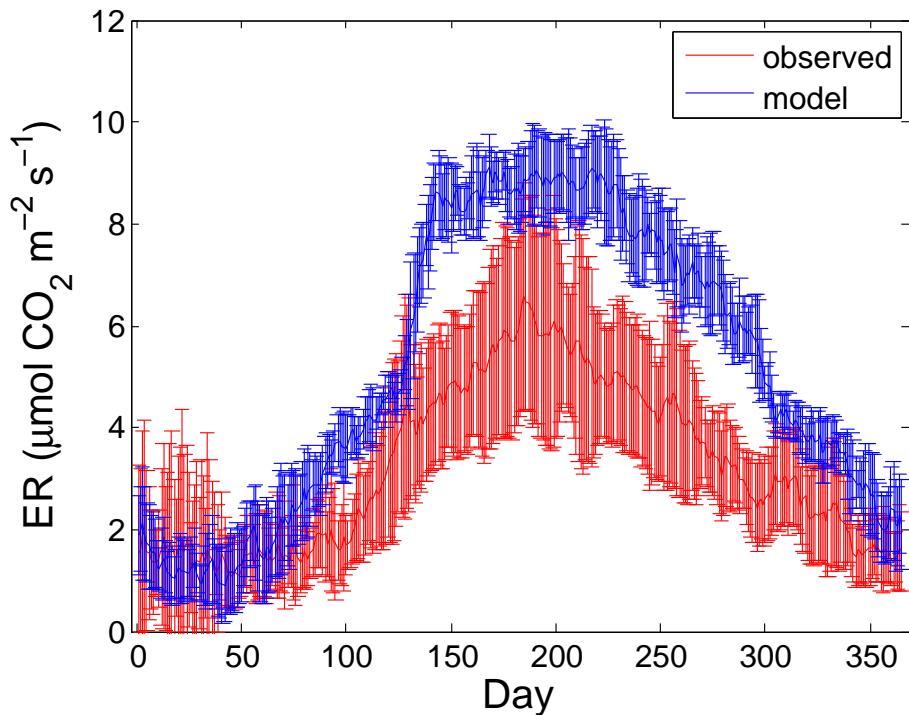


**Fig. 5.** Comparison between flux data and model simulated ecosystem respiration at the Harvard Forest site. The error bars indicate the one-standard deviation with respect to the mean. The observed data is derived from the level 4 eddy flux data at the site.

**CLM4-BeTR for biogeochemical reaction and transport**

J. Tang et al.

Title Page

Abstract Introduction

Conclusions References

Tables Figures

⏪ ⏩

◀ ▶

Back Close

Full Screen / Esc

Printer-friendly Version

Interactive Discussion



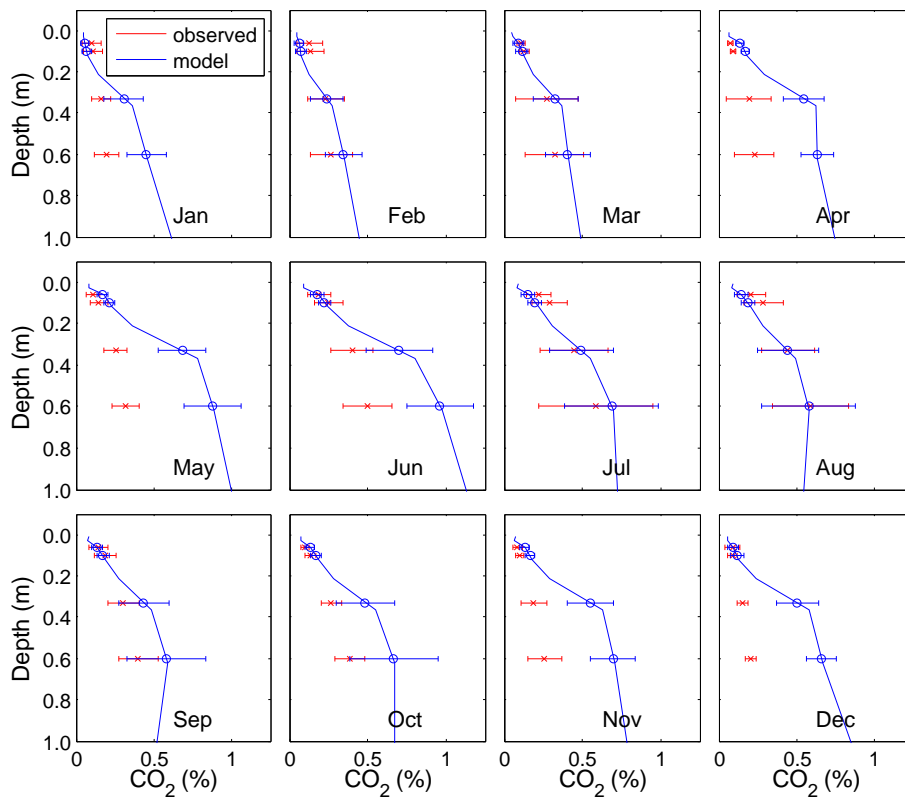


**Fig. 6.** Comparison between measured and simulated soil CO<sub>2</sub> profiles for a whole seasonal cycle. Both the measurement and model simulation were aggregated into the monthly time-step for the comparison. The error bar indicates the one-sigma standard deviation derived from all the data points in a given month.

**CLM4-BeTR for biogeochemical reaction and transport**

J. Tang et al.

[Title Page](#)  
[Abstract](#)   [Introduction](#)  
[Conclusions](#)   [References](#)  
[Tables](#)   [Figures](#)  
⏪   ⏩  
◀   ▶  
[Back](#)   [Close](#)  
[Full Screen / Esc](#)  
[Printer-friendly Version](#)  
[Interactive Discussion](#)



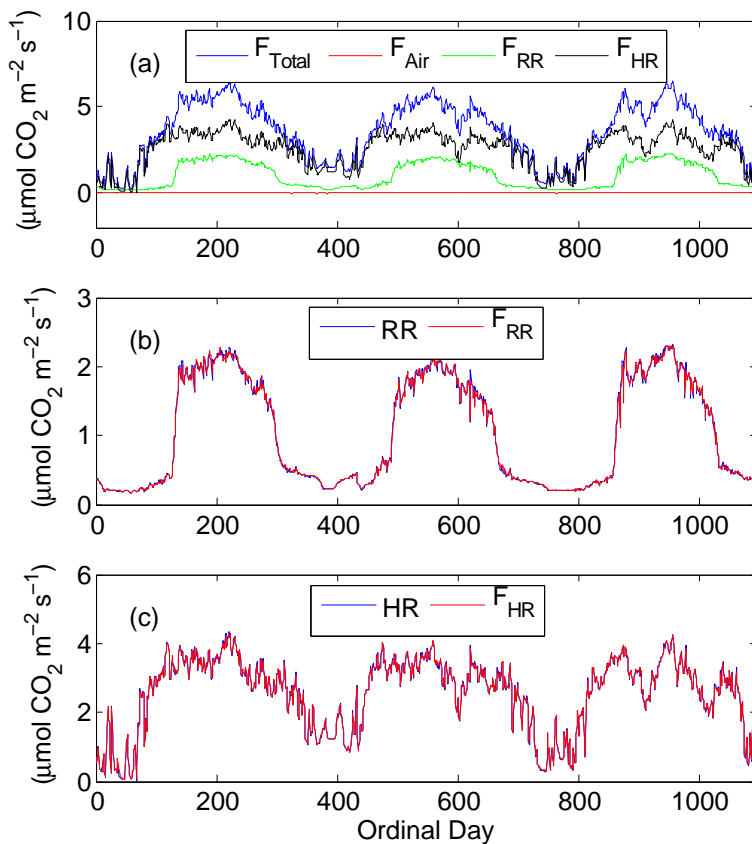


**Fig. 7.** A comparison of the simulated component-wise soil surface  $\text{CO}_2$  effluxes and their belowground production rates.  $F_{\text{Air}}$ ,  $F_{\text{RR}}$ , and  $F_{\text{HR}}$  are, respectively, the surface  $\text{CO}_2$  effluxes corresponding to atmospheric  $\text{CO}_2$  (Air), production from autotrophic root respiration (RR), and soil heterotrophic respiration (SR).  $F_{\text{total}}$  is the sum of  $F_{\text{Air}}$ ,  $F_{\text{RR}}$ , and  $F_{\text{HR}}$ .

**CLM4-BeTR for biogeochemical reaction and transport**

J. Tang et al.

Title Page

Abstract	Introduction
Conclusions	References
Tables	Figures

⏪      ⏩  
◀      ▶  
 Back      Close

Full Screen / Esc

Printer-friendly Version

Interactive Discussion



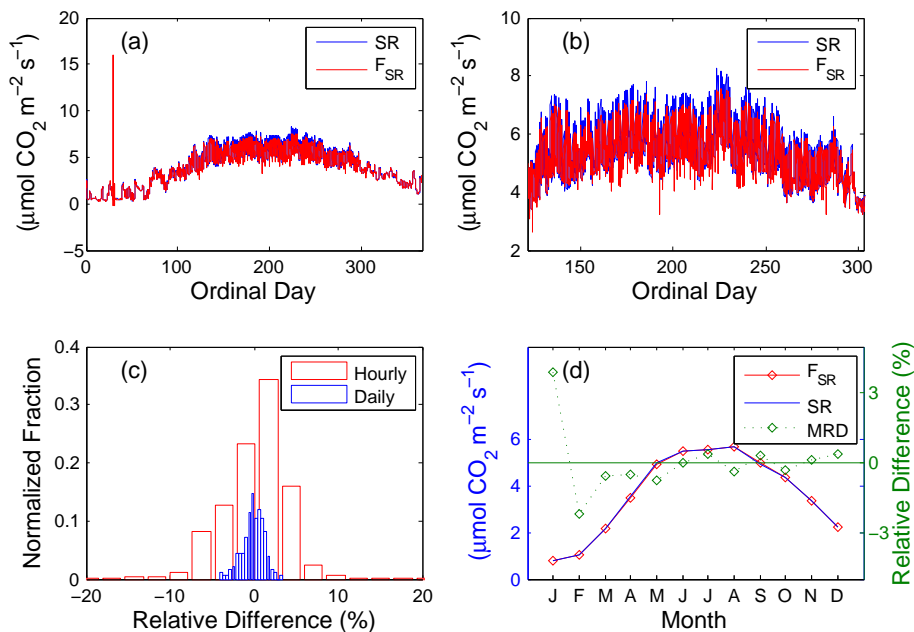


**Fig. 8.** A comparison of surface  $\text{CO}_2$  effluxes and their production rates at different temporal scales. **(a)** Comparison of hourly time series of surface  $\text{CO}_2$  efflux  $F_{\text{SR}}$  with its production from soil respiration SR, including both soil heterotrophic respiration and autotrophic root respiration. **(b)** Same as panel **(a)**, except restricted to the growing season. **(c)** Histograms of the relative differences  $((F_{\text{SR}} - \text{SR}) / F_{\text{SR}} \times 100\%)$  at hourly and daily time steps. **(d)** Comparison of monthly time step time series of surface  $\text{CO}_2$  effluxes and soil respiration. MRD represents the monthly relative difference. See text for details of the analysis

[Title Page](#)
[Abstract](#)
[Introduction](#)
[Conclusions](#)
[References](#)
[Tables](#)
[Figures](#)
[Back](#)
[Close](#)
[Full Screen / Esc](#)
[Printer-friendly Version](#)
[Interactive Discussion](#)

CLM4-BeTR for  
biogeochemical  
reaction and  
transport

J. Tang et al.

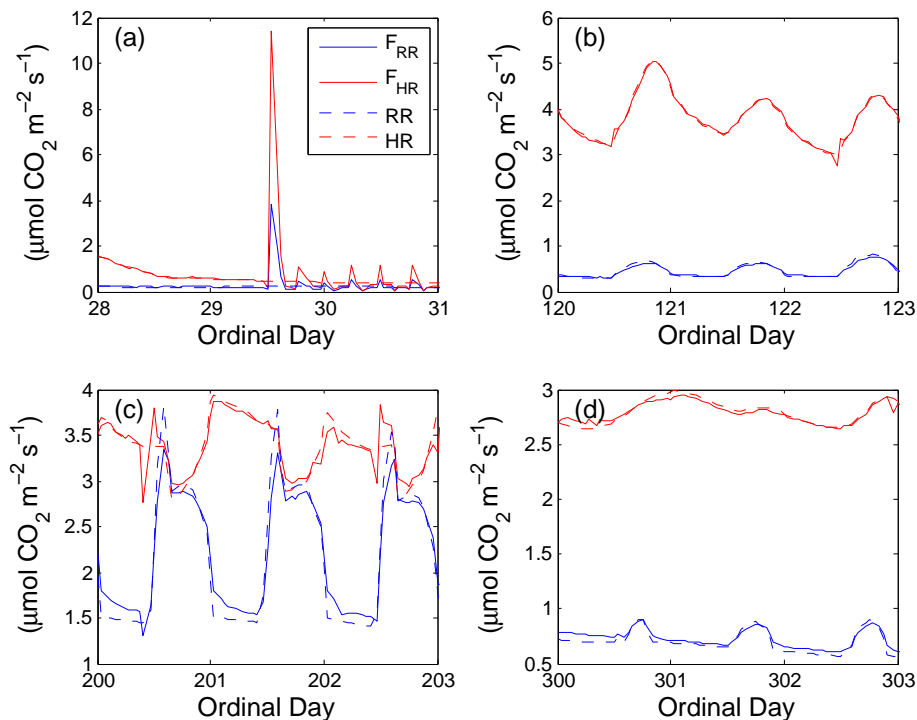


**Fig. 9.** Comparison of simulated surface  $\text{CO}_2$  efflux with their corresponding belowground production rates at four different time periods.  $F_{\text{RR}}$  is the surface  $\text{CO}_2$  efflux corresponding to that produced from autotrophic root respiration RR.  $F_{\text{HR}}$  is the surface  $\text{CO}_2$  efflux corresponding to that produced from soil heterotrophic respiration HR.

Title Page

Abstract

Introduction

Conclusions

References

Tables

Figures

◀

▶

◀

▶

Back

Close

Full Screen / Esc

Printer-friendly Version

Interactive Discussion

CLM4-BeTR for  
biogeochemical  
reaction and  
transport

J. Tang et al.

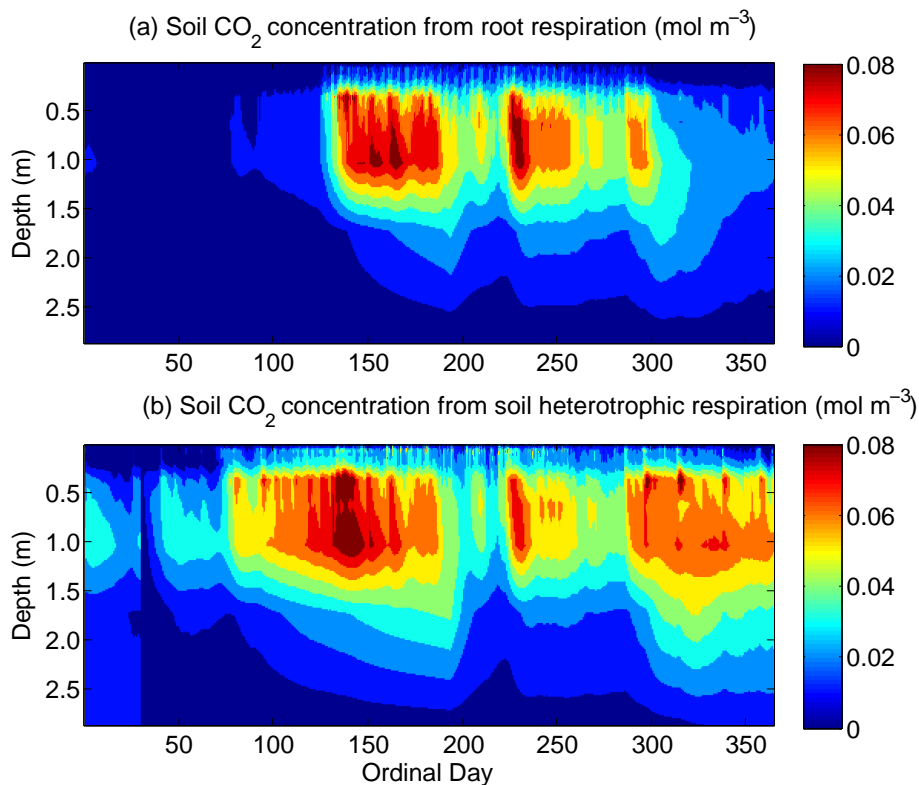


**Fig. 10.** Simulated seasonal cycle of soil CO<sub>2</sub> concentrations contributed from **(a)** autotrophic root respiration and **(b)** soil heterotrophic respiration.

[Title Page](#)[Abstract](#)[Introduction](#)[Conclusions](#)[References](#)[Tables](#)[Figures](#)[⏪](#)[⏩](#)[◀](#)[▶](#)[Back](#)[Close](#)[Full Screen / Esc](#)[Printer-friendly Version](#)[Interactive Discussion](#)